*polymers*

*Supplementary Information*

# Eight-Fold Interpenetrating Diamondoid Coordination Polymers for Sensing Volatile Organic Compounds and Metal Ions

**Venkatesan Lakshmanan [1], Yi-Ting Lai [1], Xiang-Kai Yang [1], Manivannan Govindaraj [1], Chia-Her Lin [2,*] and Jhy-Der Chen [1,*]**

[1] Department of Chemistry, Chung-Yuan Christian University, Chung Li 32023, Taiwan; venkatesanflower95@gmail.com (V.L.); e0912583362@gmail.com (Y.-T.L.); xiangkaishulin@gmail.com (X.-K.Y.); manivannanjent@gmail.com (M.G.)
[2] Department of Chemistry, National Taiwan Normal University, Taipei 11677, Taiwan
[*] Correspondence: chiaher@ntnu.edu.tw (C.-H.L.); jdchen@cycu.edu.tw (J.-D.C.); Tel.: +886-3-265-3351 (J.-D.C.)

**Citation:** Lakshmanan, V.; Lai, Y.-T.; Yang, X.-K.; Govindaraj, M.; Lin, C.-H. Eight-Fold Interpenetrating Diamondoid Coordination Polymers for Sensing Volatile Organic Compounds and Metal Ions. *Polymers* **2021**, *13*, x. https://doi.org/10.3390/xxxxx

Academic Editor:

Received: date
Accepted: date
Published: date



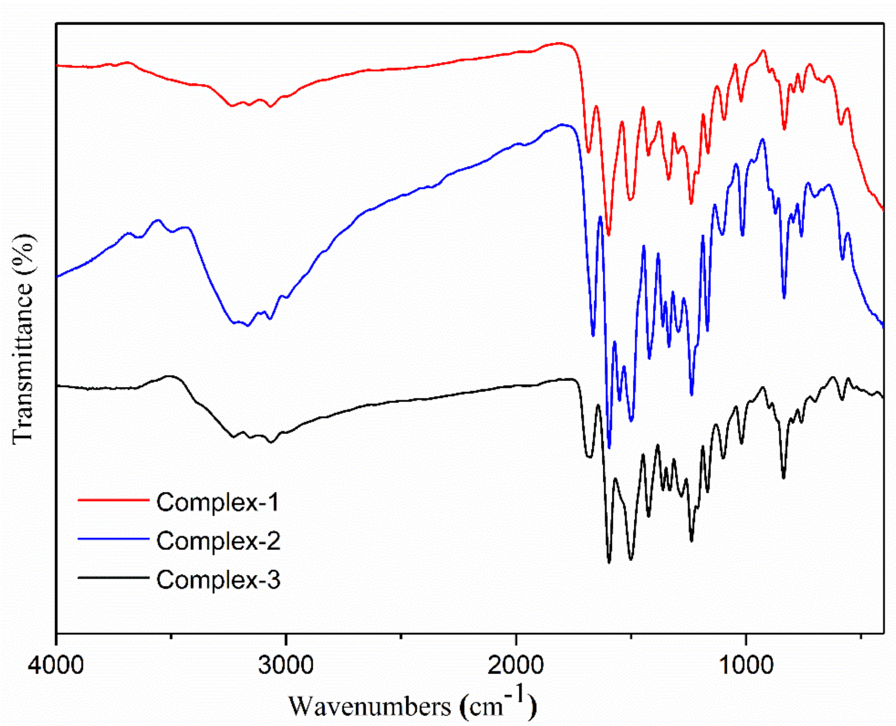


**Figure S1.** FT-IR spectra of complexes 1 - 3.

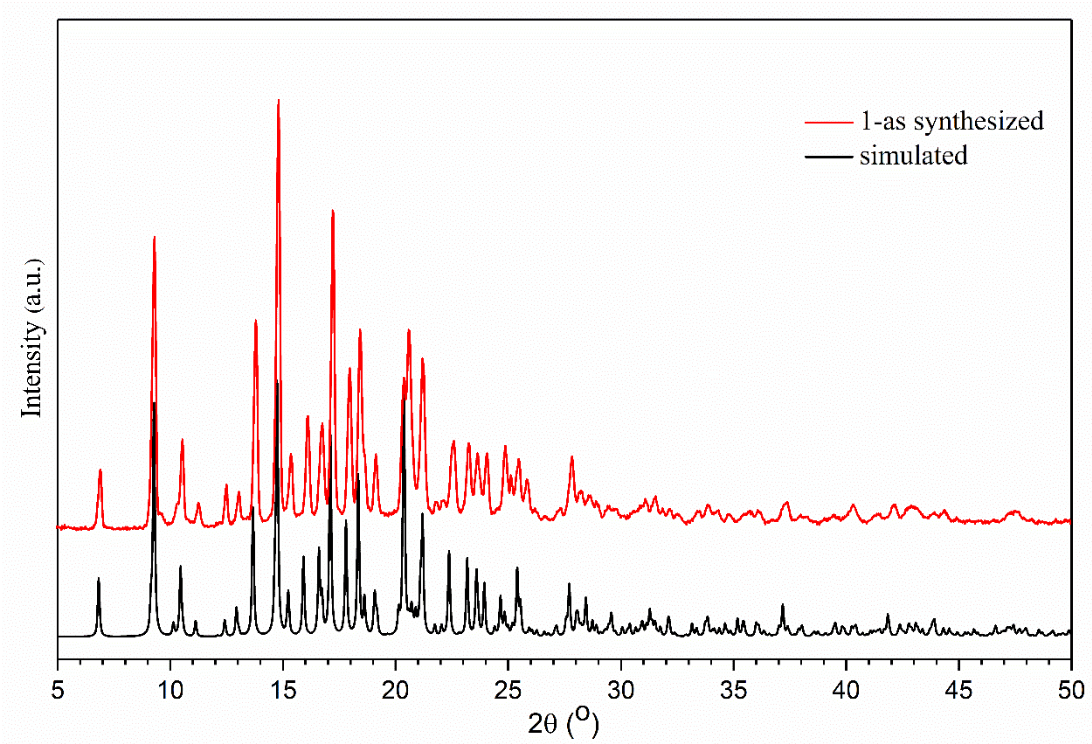


**Figure S2.** PXRD patterns of 1.

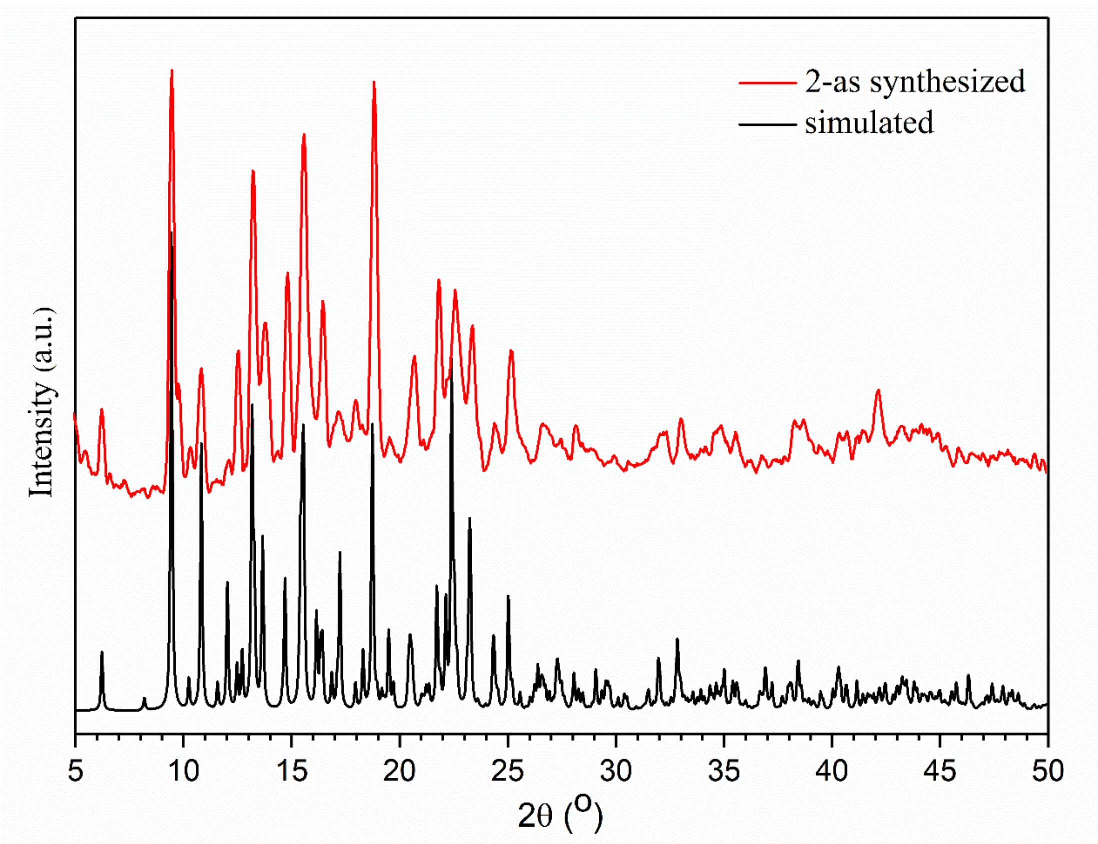


**Figure S3.** PXRD patterns of **2**.

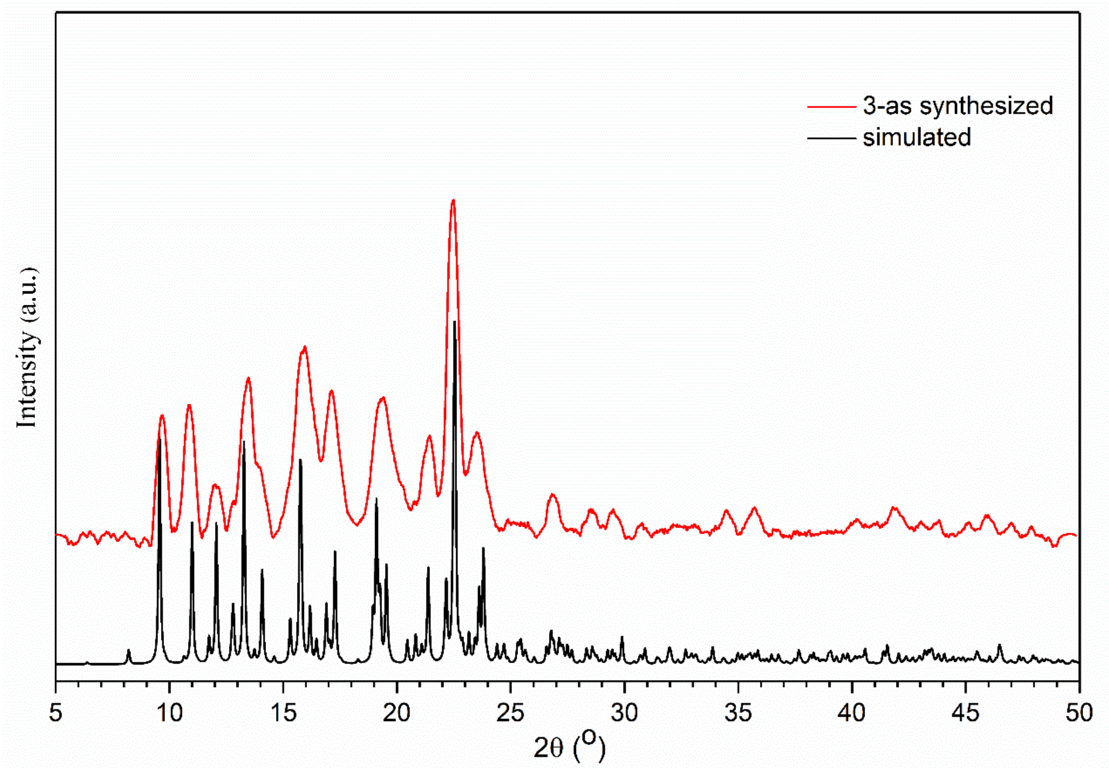


**Figure S4.** PXRD patterns of **3**.

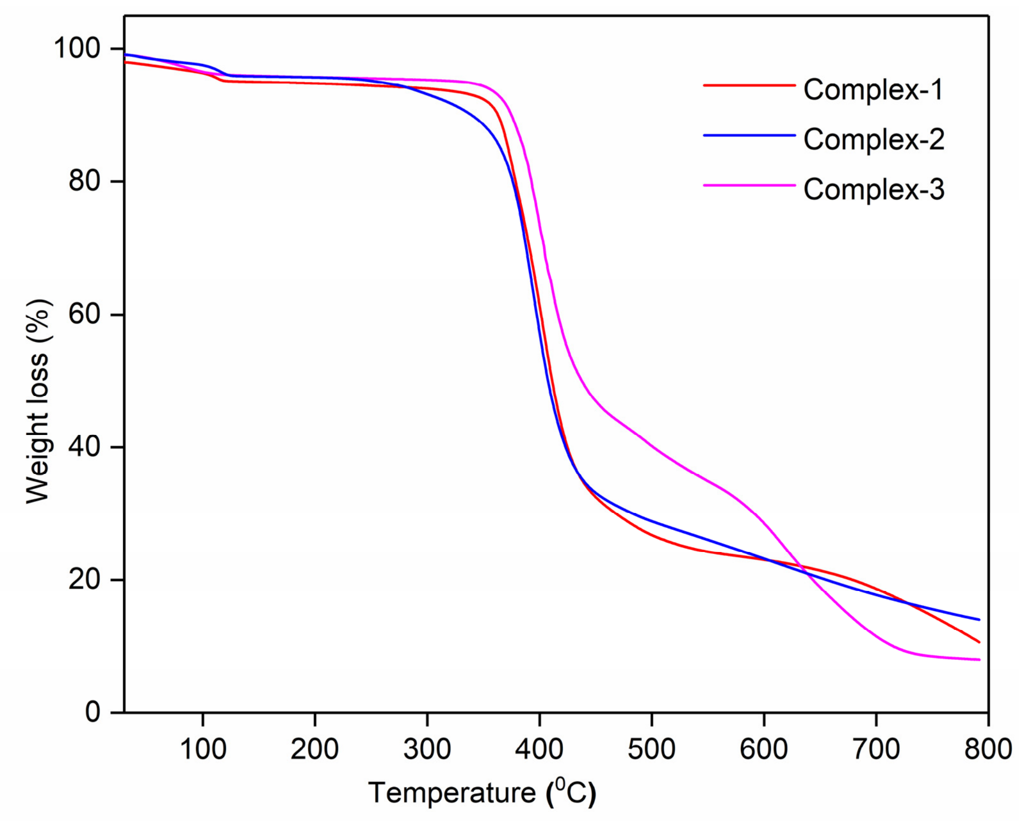


**Figure S5.** TGA curves for complexes **1** (red), **2** (blue) and **3** (magenta).

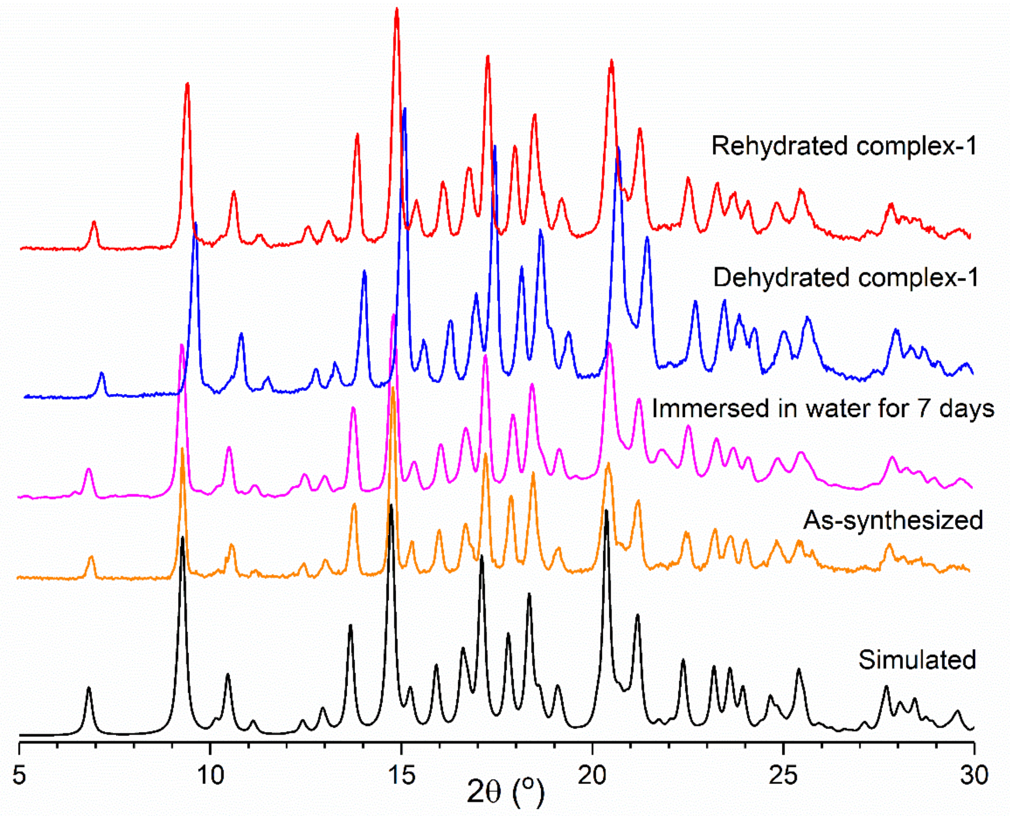


**Figure S6.** PXRD patterns of the dehydrated and rehydrated **1**.

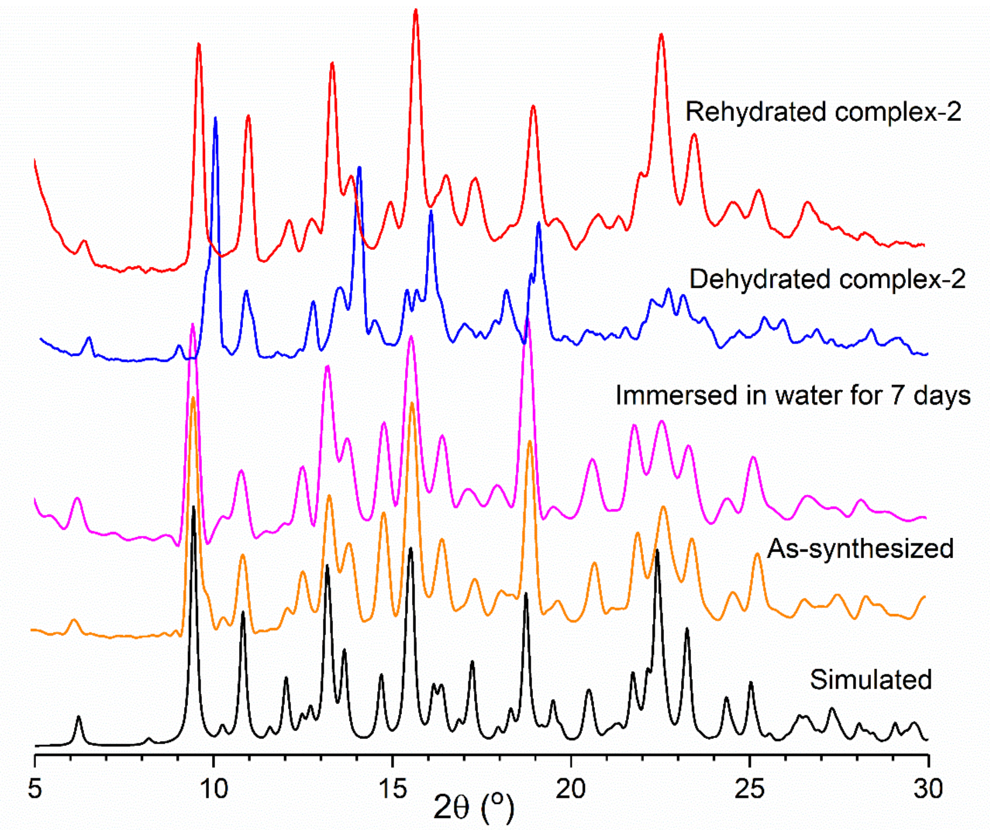


**Figure S7.** PXRD patterns of the dehydrated and rehydrated **2**.

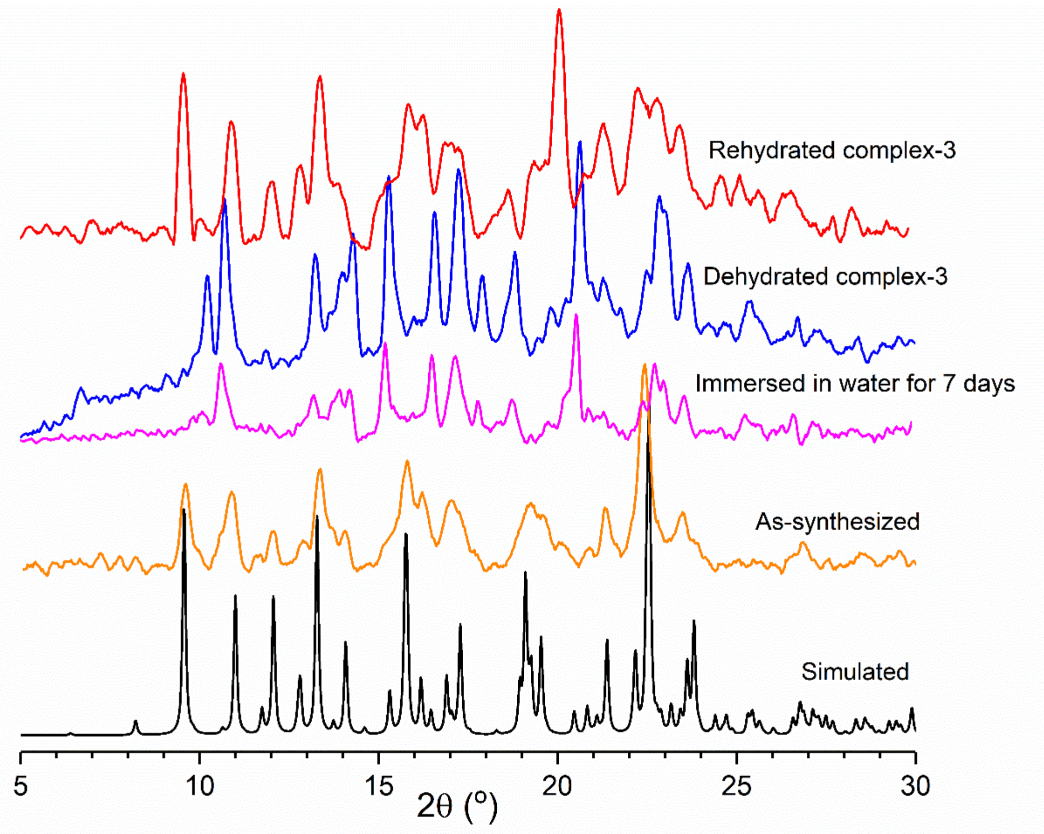


**Figure S8.** PXRD patterns of the dehydrated and rehydrated **3**.

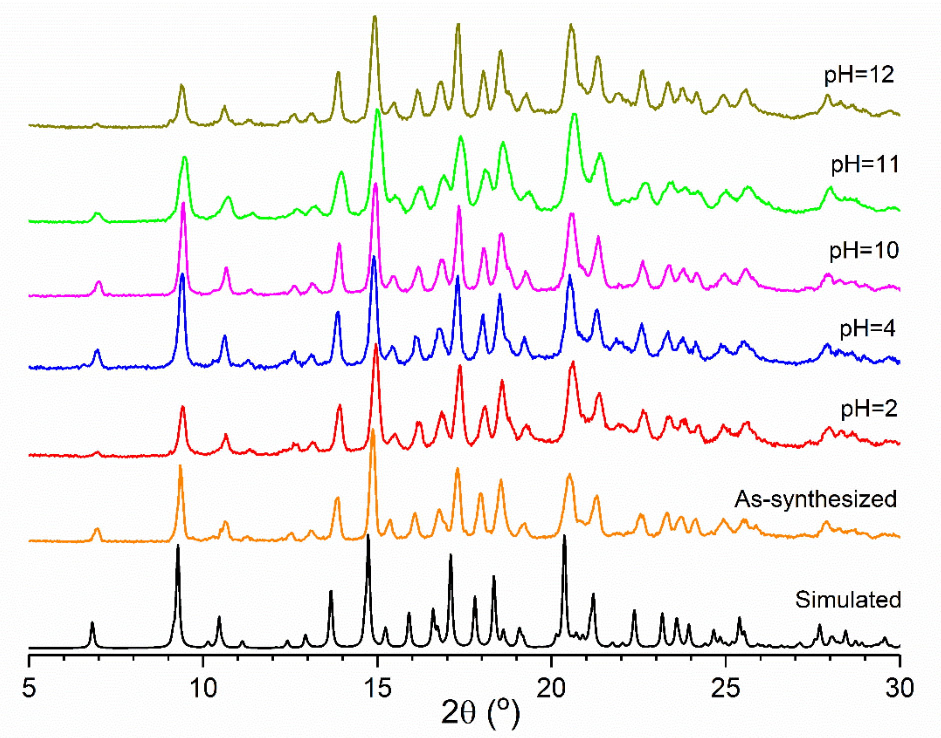


**Figure S9.** PXRD patterns of complex **1** in various pH values.

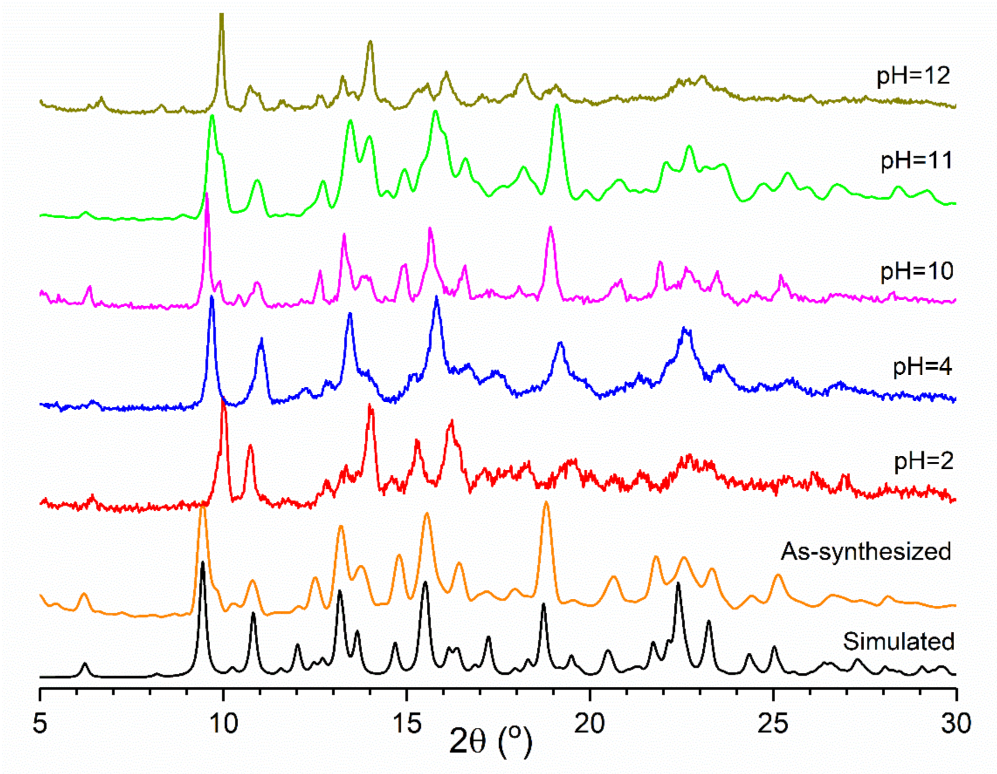


**Figure S10.** PXRD patterns of complex **2** in various pH values.

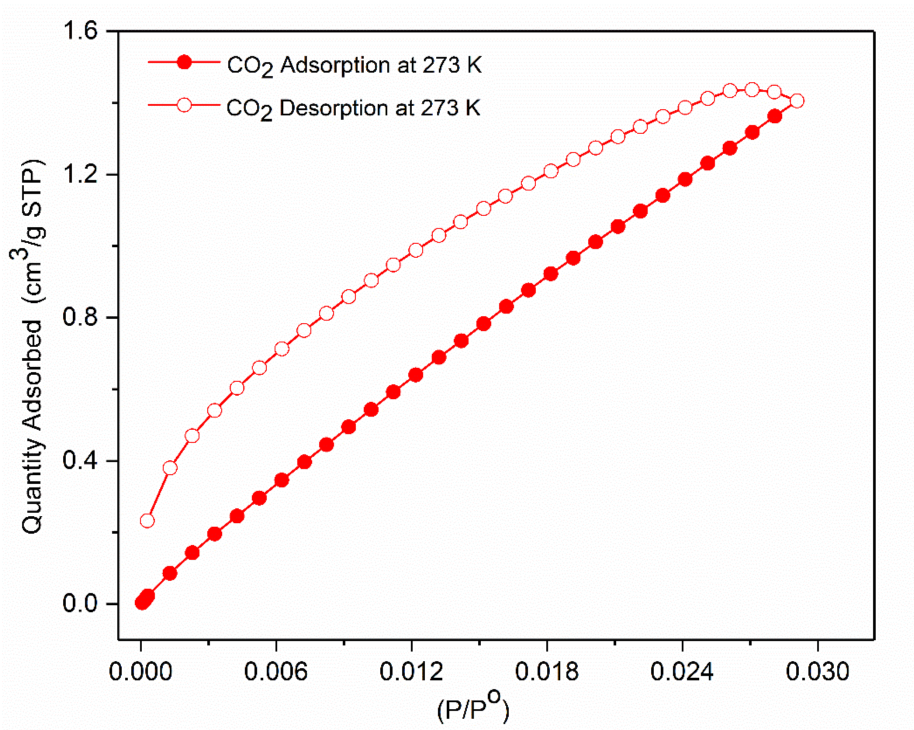


**(a).**

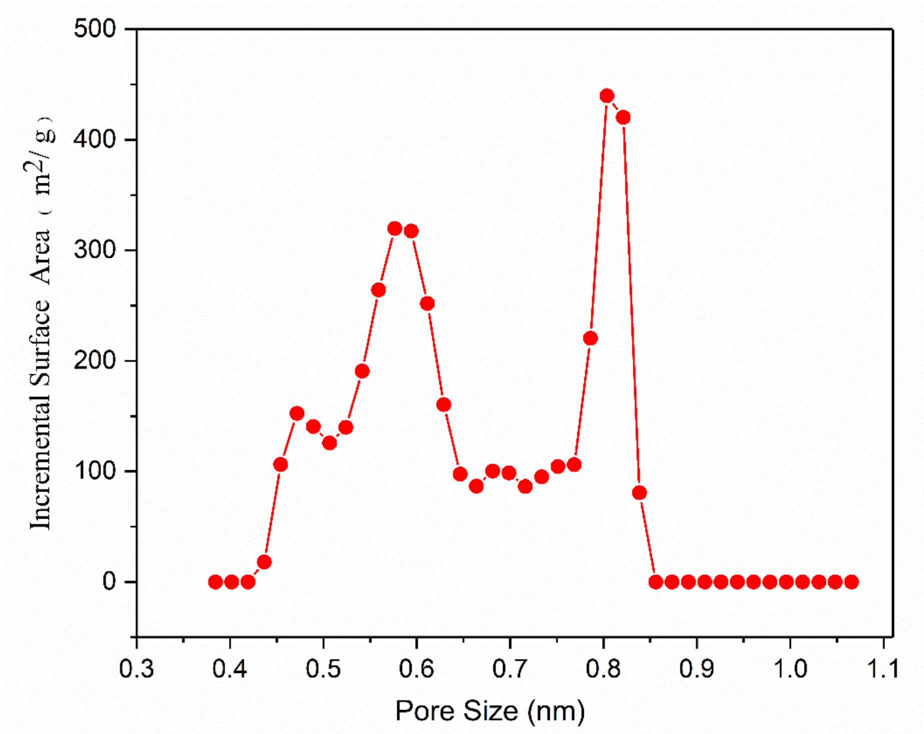


**(b).**

**Figure 11.** (**a**) $CO_2$ sorption isotherm of complex **1** at 273 K and (**b**) pore size distributions.

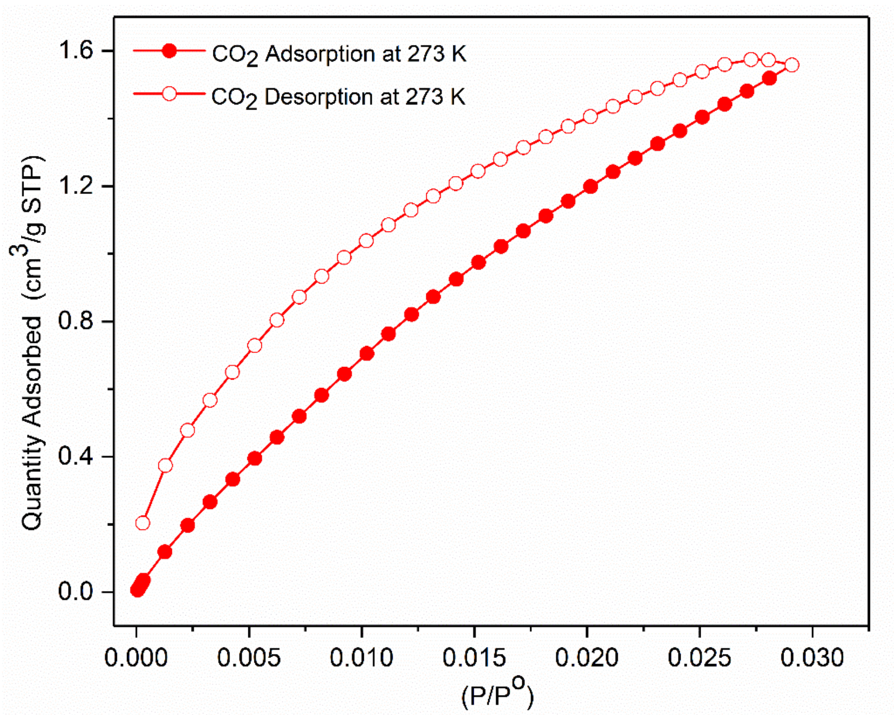


**(a).**

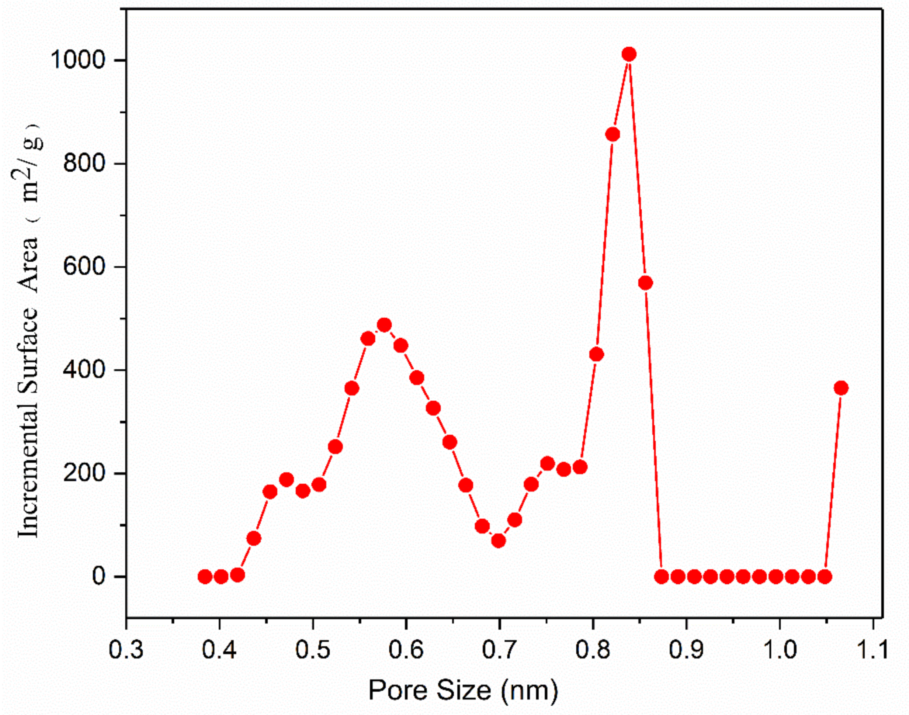


**(b).**

**Figure S12.** (**a**) $CO_2$ sorption isotherm of complex **2** at 273 K and (**b**) pore size distributions.

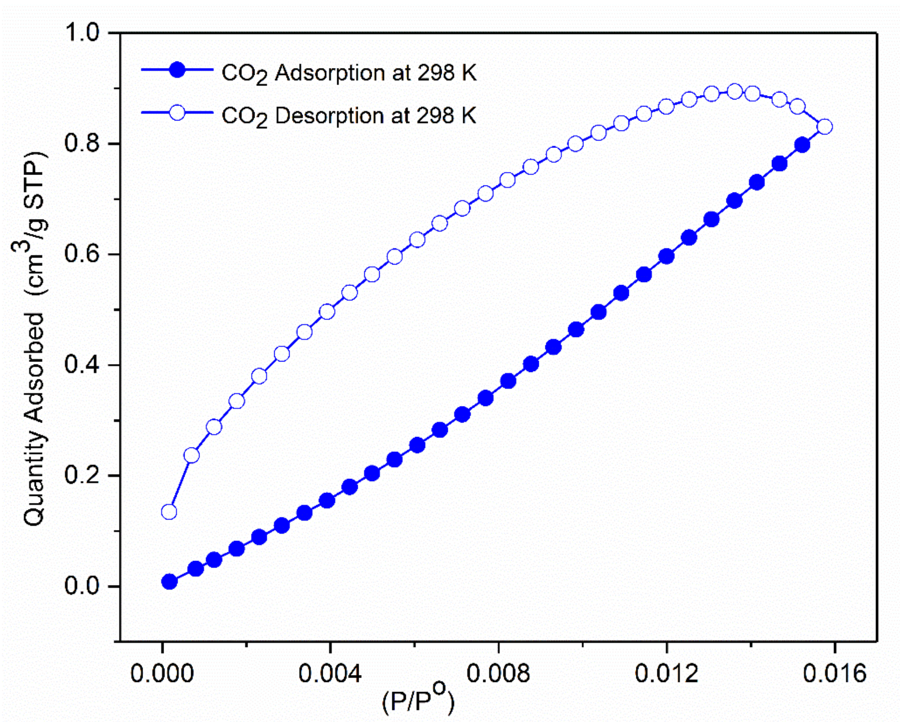


**(a).**

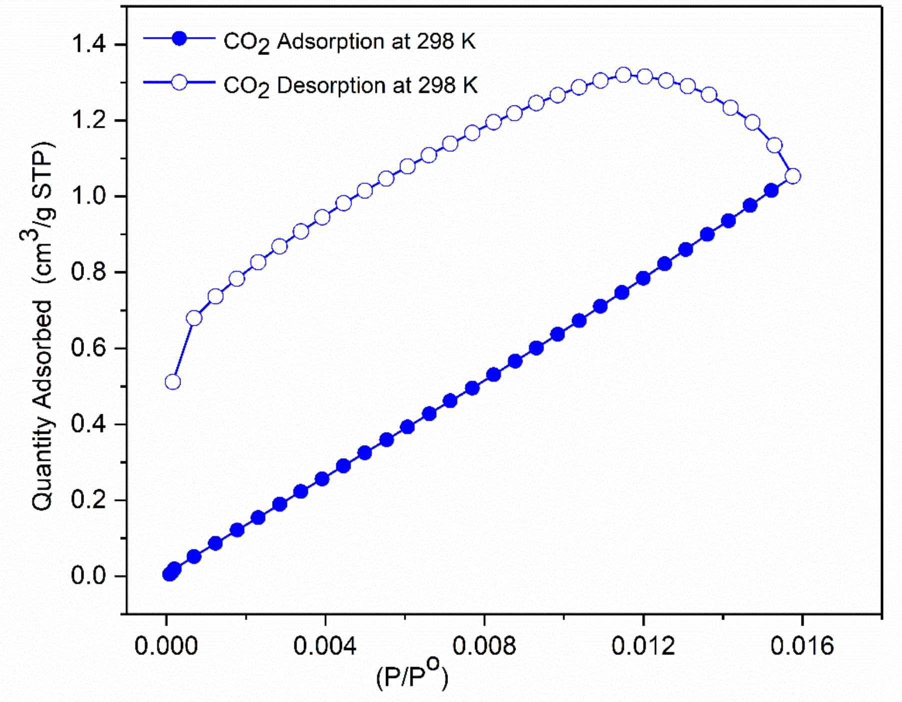

CO2 Adsorption at 298 K
CO2 Desorption at 298 K
Quantity Adsorbed (cm3/g STP)
(P/P0)
1.4
1.2
1.0
0.8
0.6
0.4
0.2
0.0
0.000
0.004
0.008
0.012
0.016


**(b).**

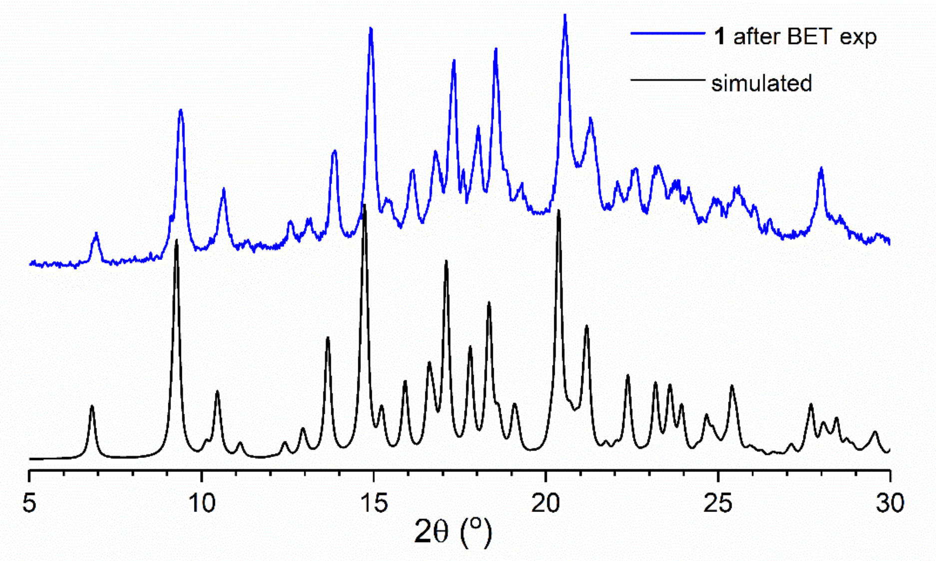

1 after BET exp
simulated
2θ (°)
5
10
15
20
25
30


**(c).**

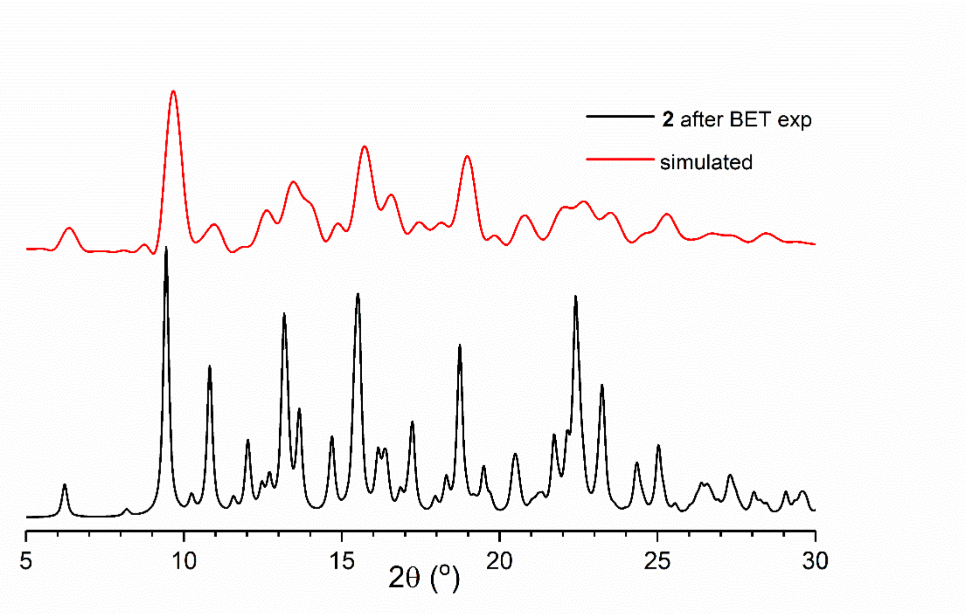


**(d).**

**Figure S13.** $CO_2$ sorption isotherms of complexes (**a**) **1** and (**b**) **2** at 298 K and PXRD patterns of (**c**) **1** and (**d**) **2** measured after experiments.

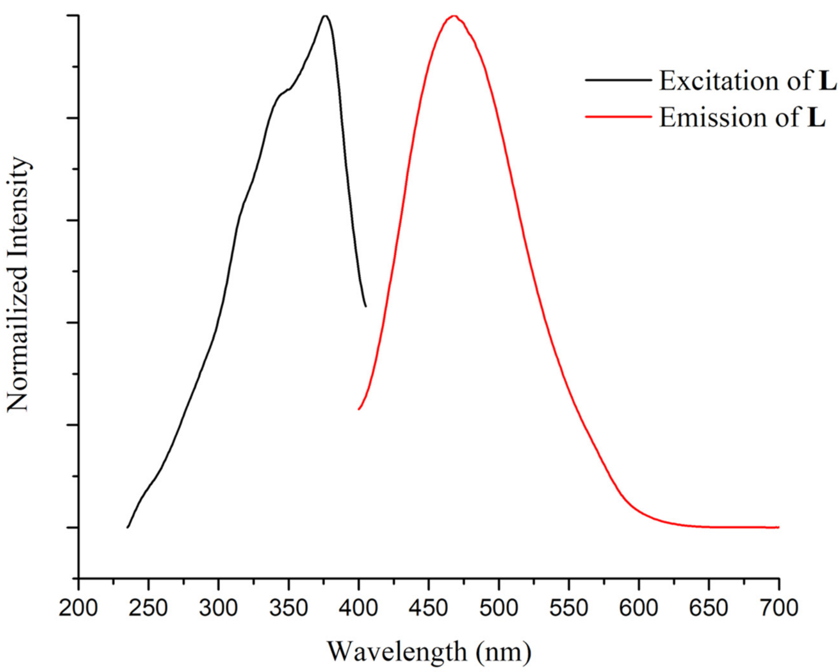


**(a).**

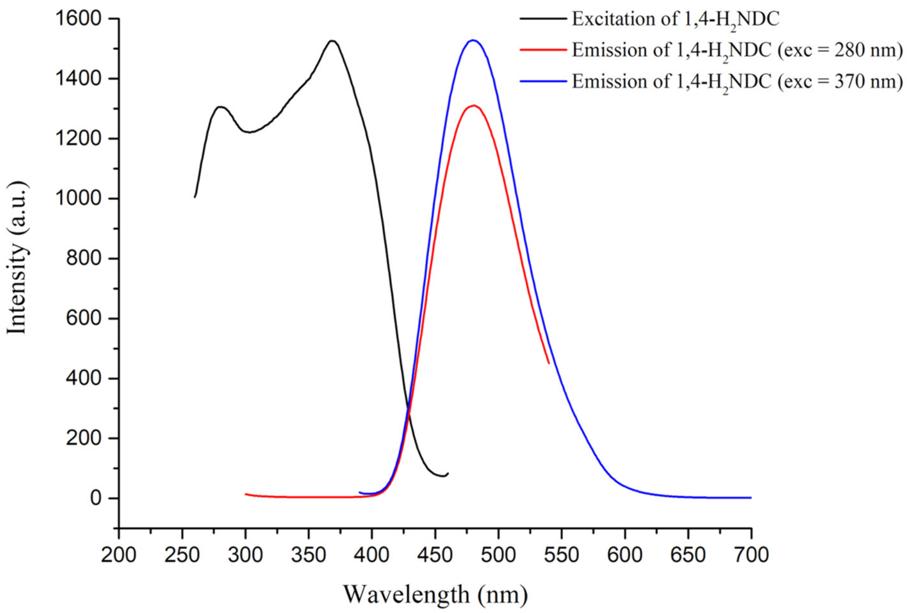


**(b).**

**Figure S14.** (**a**) Emission spectra of ligand **L** and (**b**) emission spectra of 1,4-$H_2NDC$.

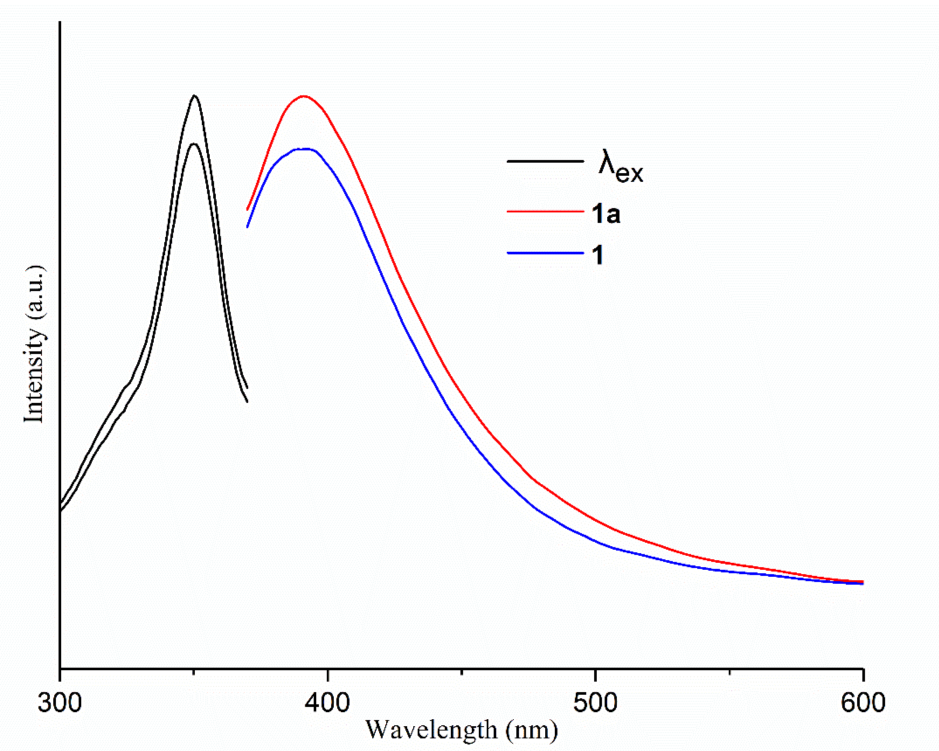


**(a).**

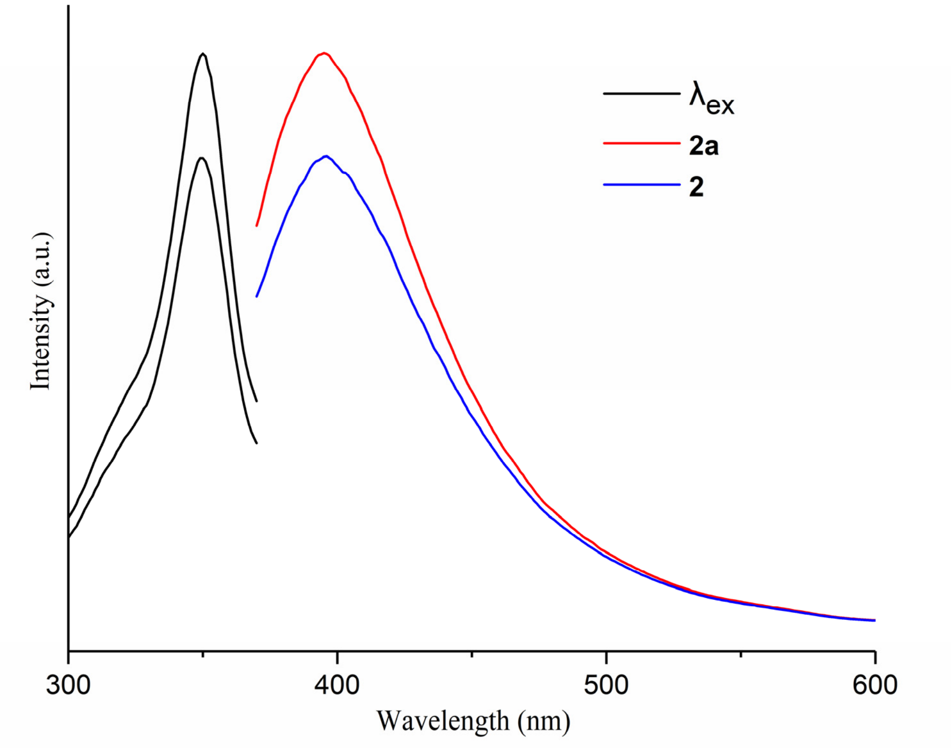


**(b).**

**Figure S15.** Emission spectra of (**a**) complex **1** and **1a** and (**b**) complex **2** and **2a**.

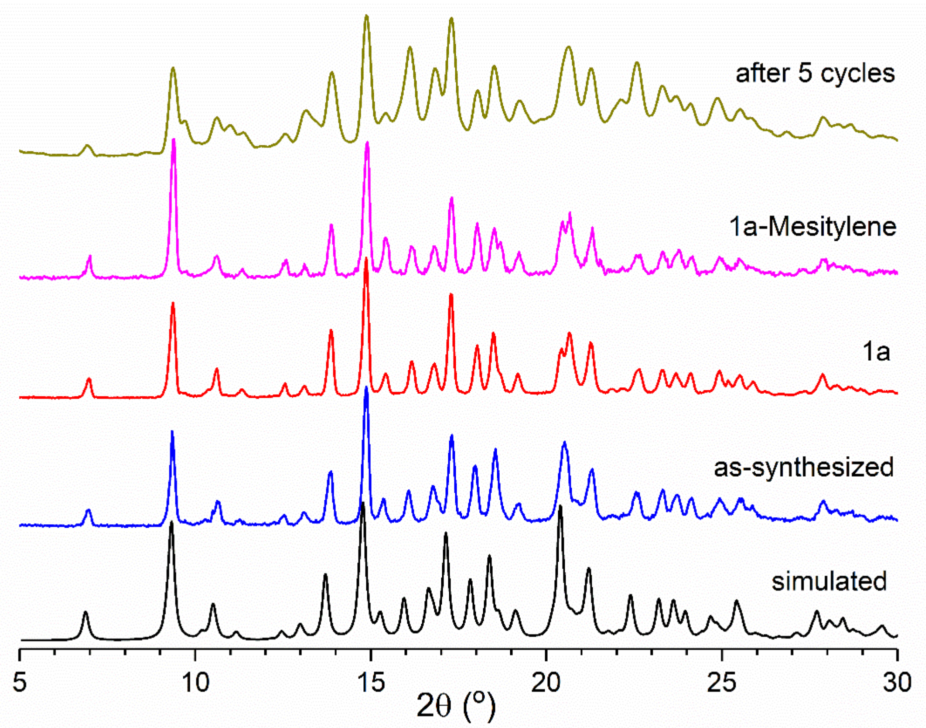


**(a).**

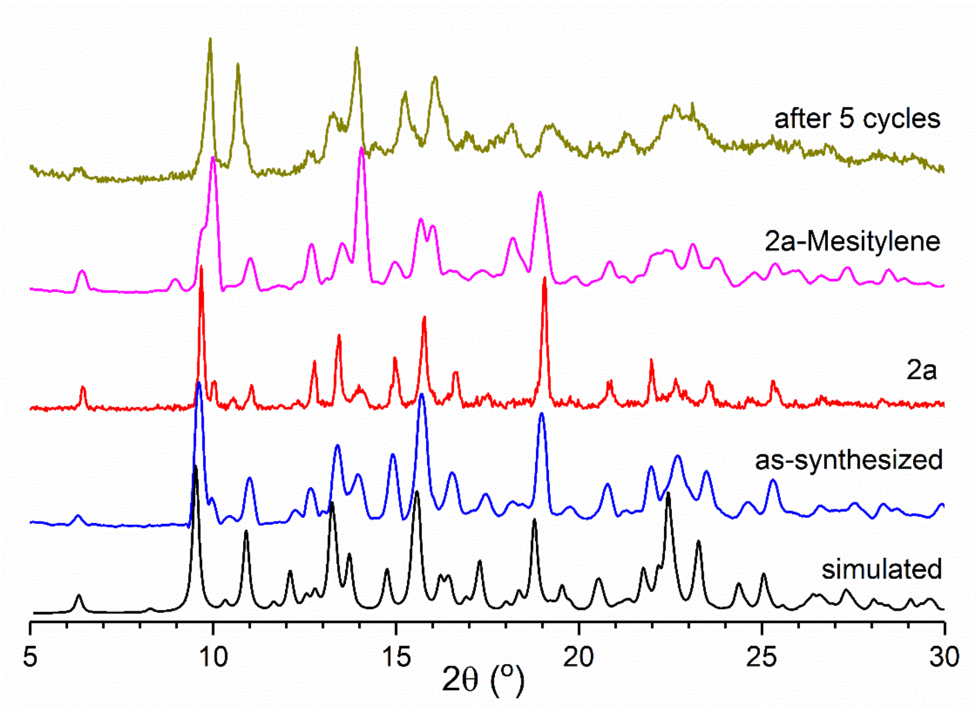


**(b).**

**Figure S16.** PXRD patterns for (a) **1a** and (b) **2a** before and after exposure with mesitylene.

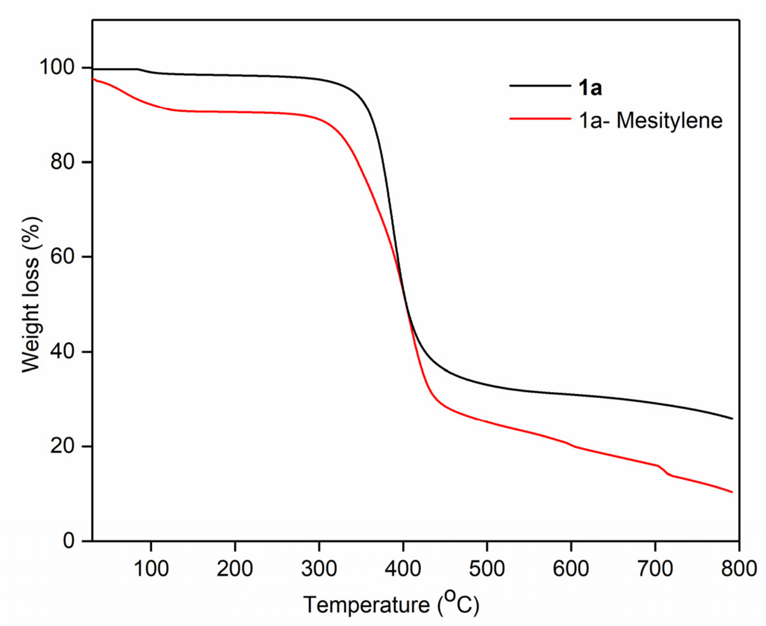


**(a).**

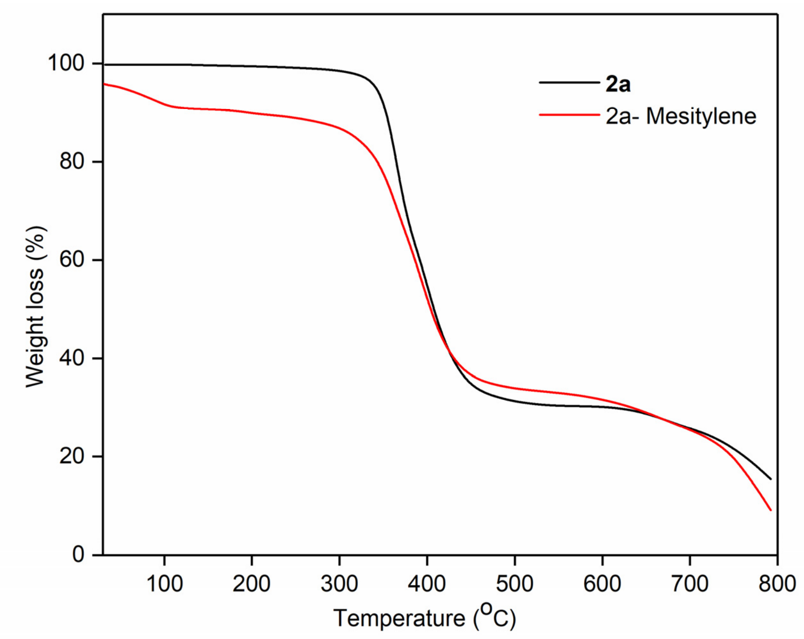


**(b).**

**Figure S17.** TGA curves measured for (a) **1a** and mesitylene-loaded **1a** and (b) **2a** and mesitylene-loaded **2a**.

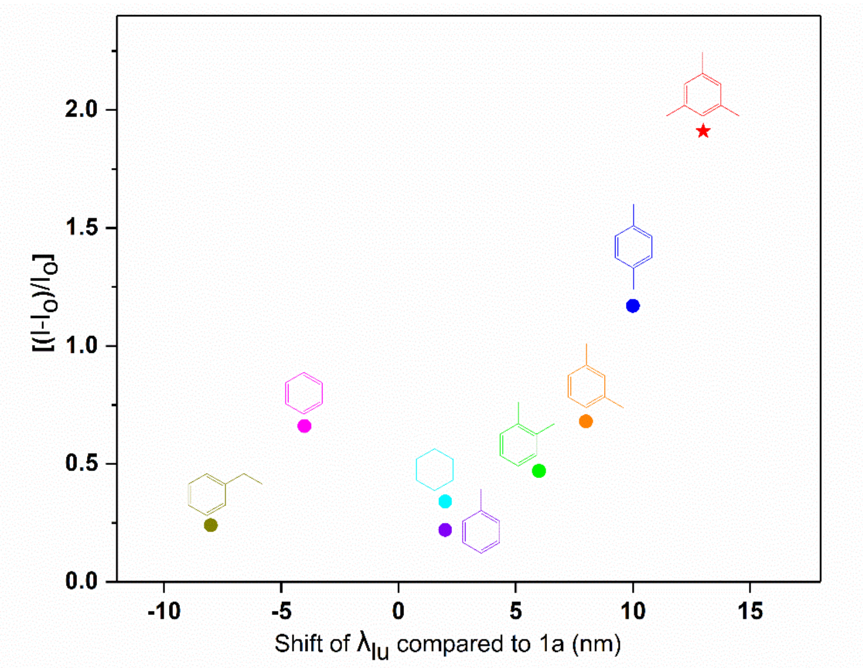


**(a).**

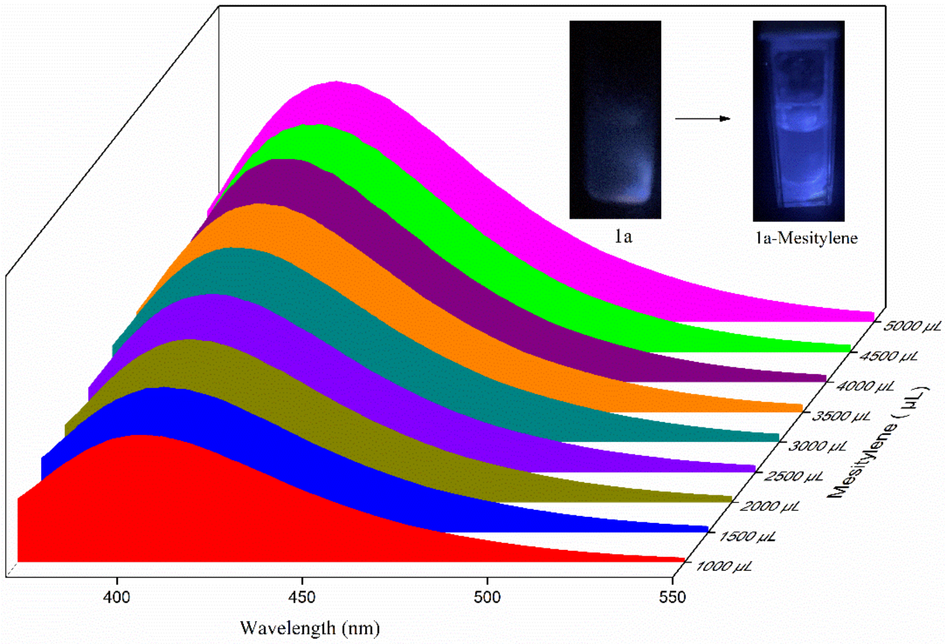


**(b).**

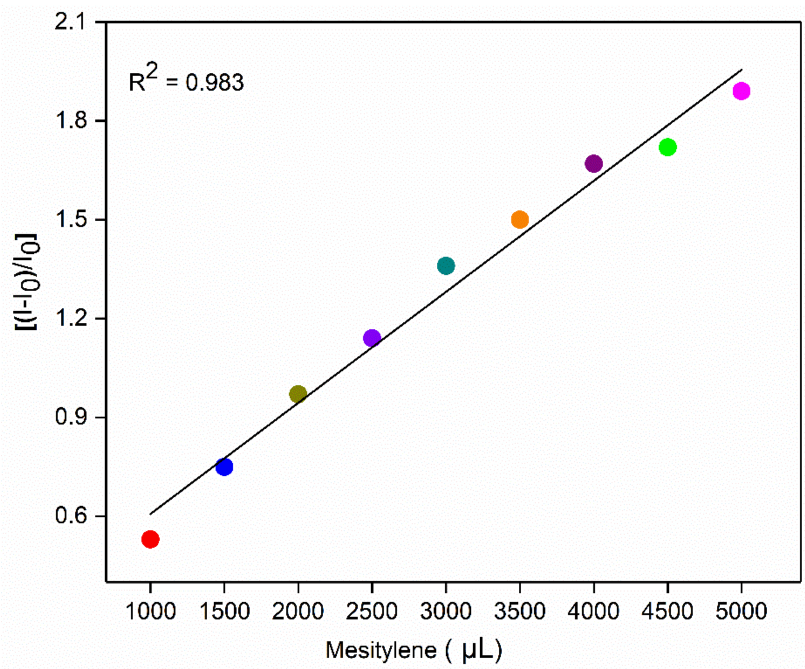


**(c).**

**Figure S18.** (a) The relationship of luminescence intensities of VOCs-loaded **1a** versus emission wavelength shifts of $\lambda_{lu}$ compared to **1a**. (b) Emission spectra of **1a** with increasing amount of mesitylene upon excitation at 350 nm. (c) The calibration curves showing luminescence intensity of **1a** at different amount of mesitylene.

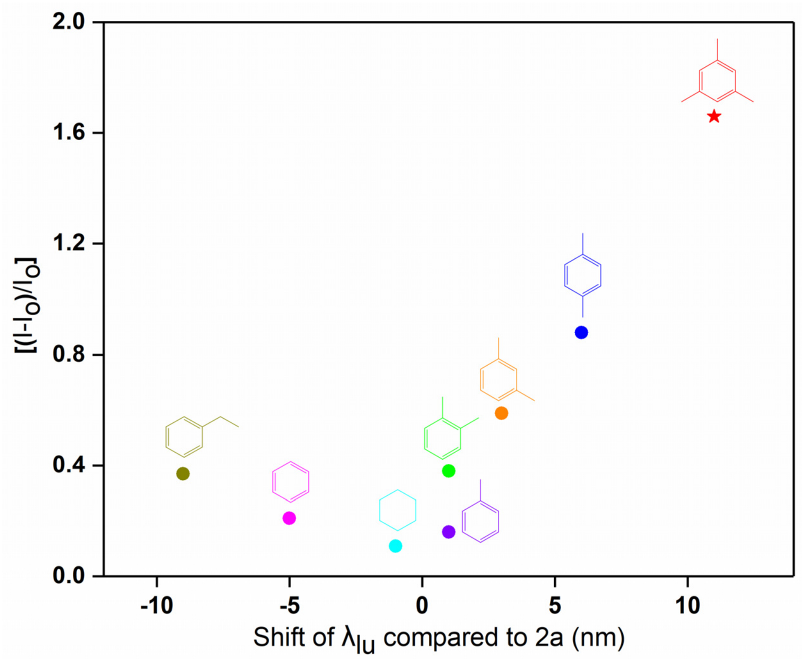

2.0
1.6
1.2
0.8
0.4
0.0
[(I-I$_O$)/I$_O$]
-10
-5
0
5
10
Shift of λ$_{lu}$ compared to 2a (nm)


**(a).**

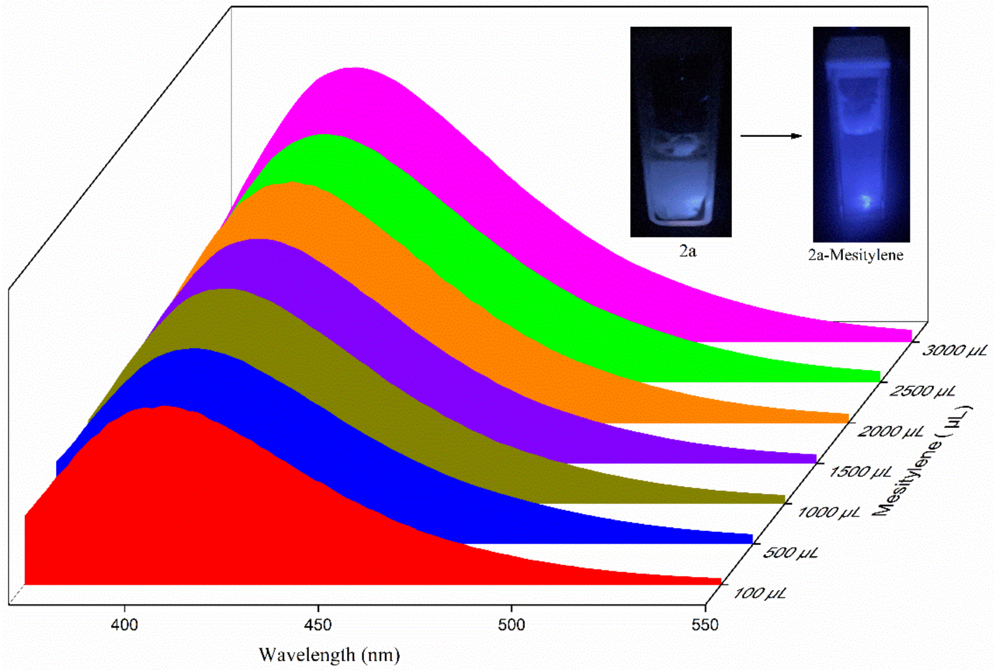

2a
2a-Mesitylene
3000 μL
2500 μL
2000 μL
1500 μL
1000 μL
500 μL
100 μL
Mesitylene ( μL)
400
450
500
550
Wavelength (nm)


**(b).**

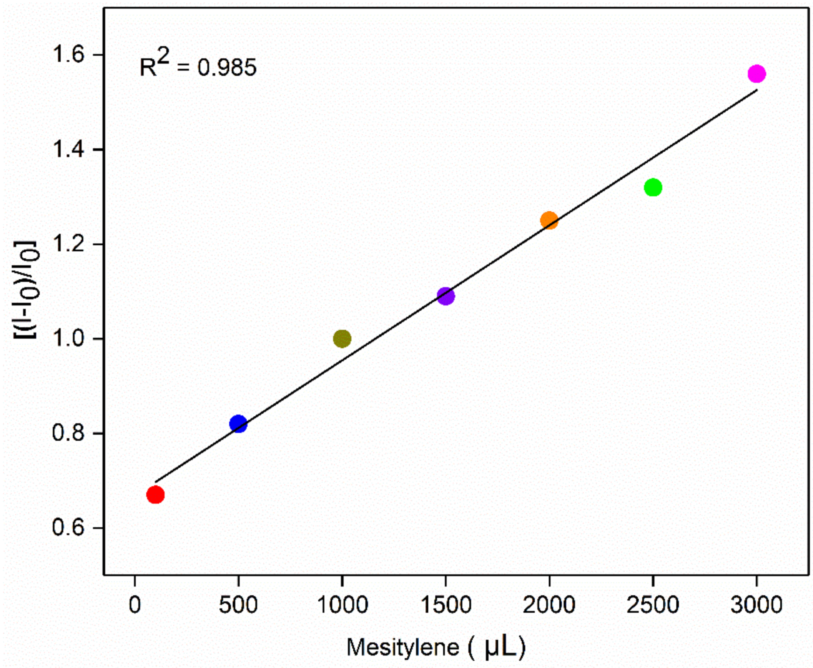


**(c).**

**Figure S19.** (a) The relationship of luminescence intensities of VOCs-loaded **2a** versus emission wavelength shifts of $\lambda_{lu}$ compared to **2a**. (b) Emission spectra of **2a** with increasing amount of mesitylene upon excitation at 350 nm. (c) The calibration curves showing luminescence intensity of **2a** at different amount of mesitylene.

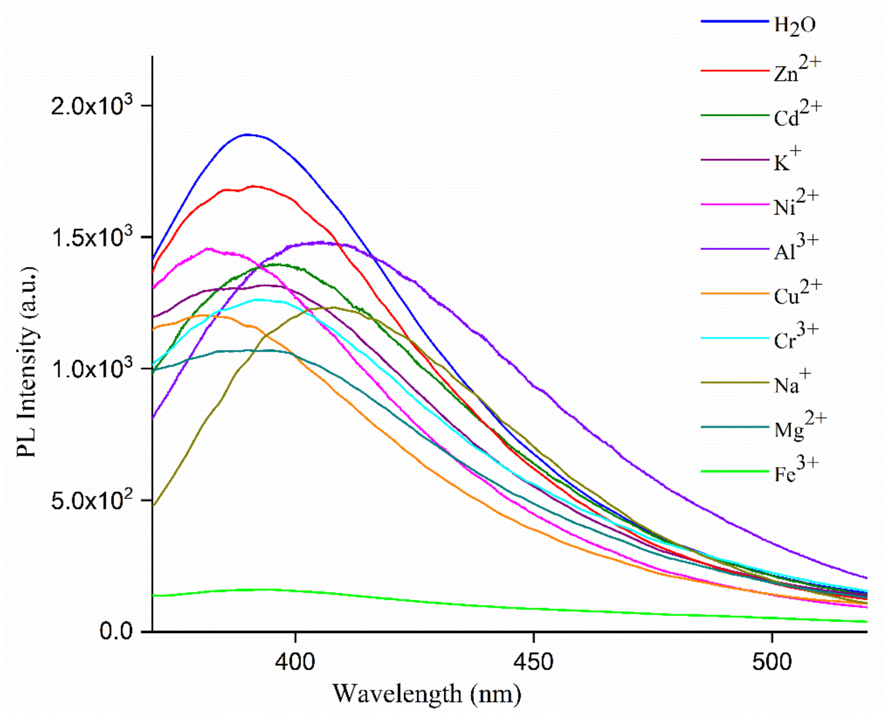


**(a).**

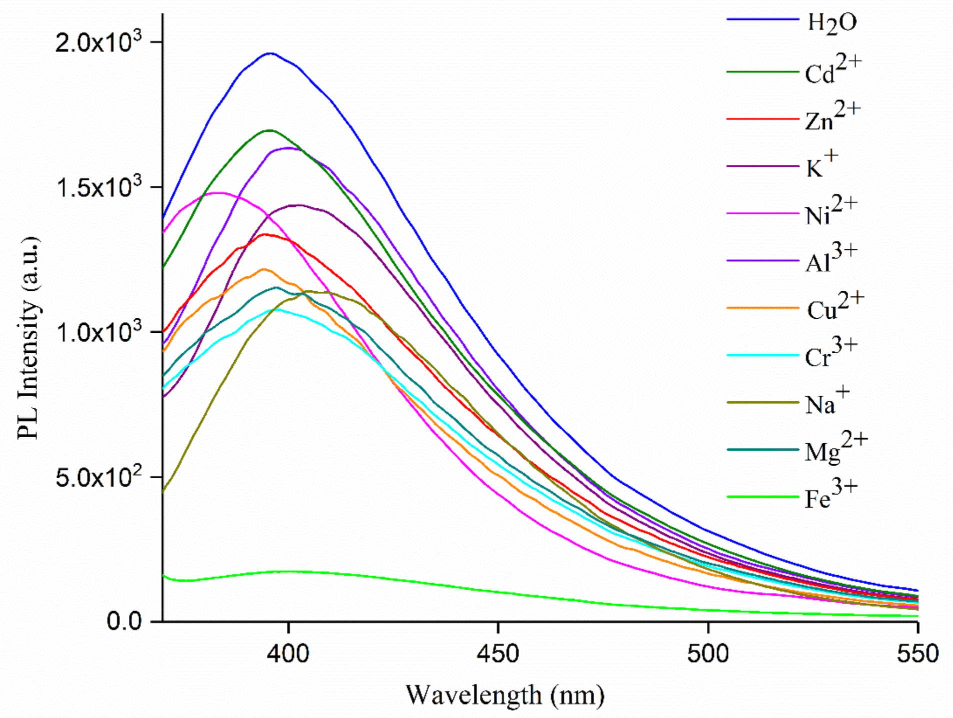


**(b).**

**Figure S20.** Luminescence responses towards aqueous solutions of various metal cations upon excitation at 350 nm for (a) **1** and (b) **2**.

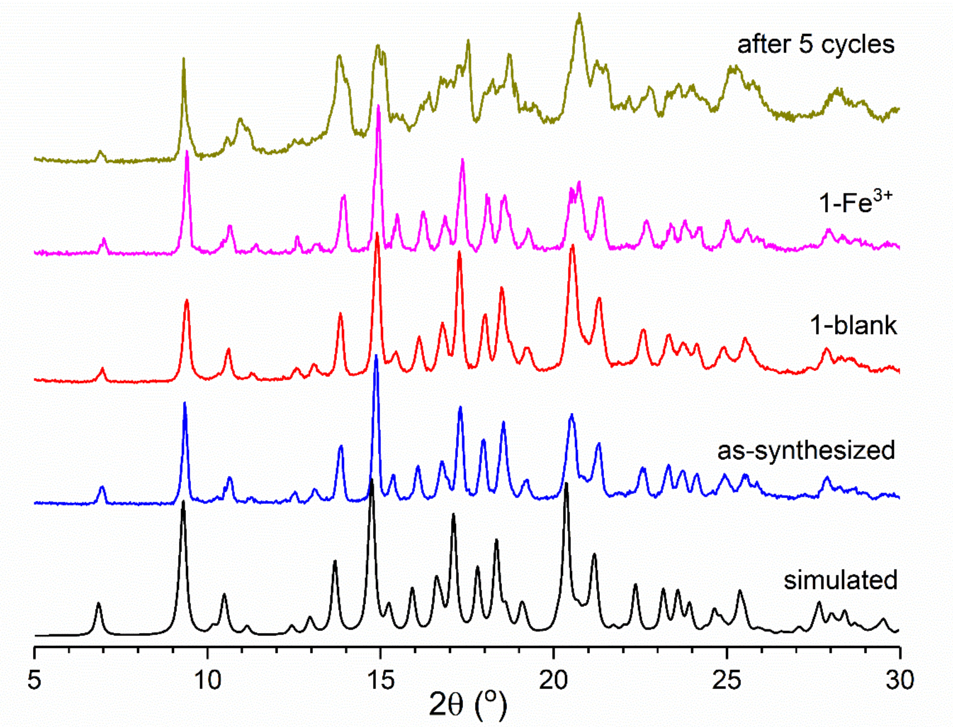


**(a).**

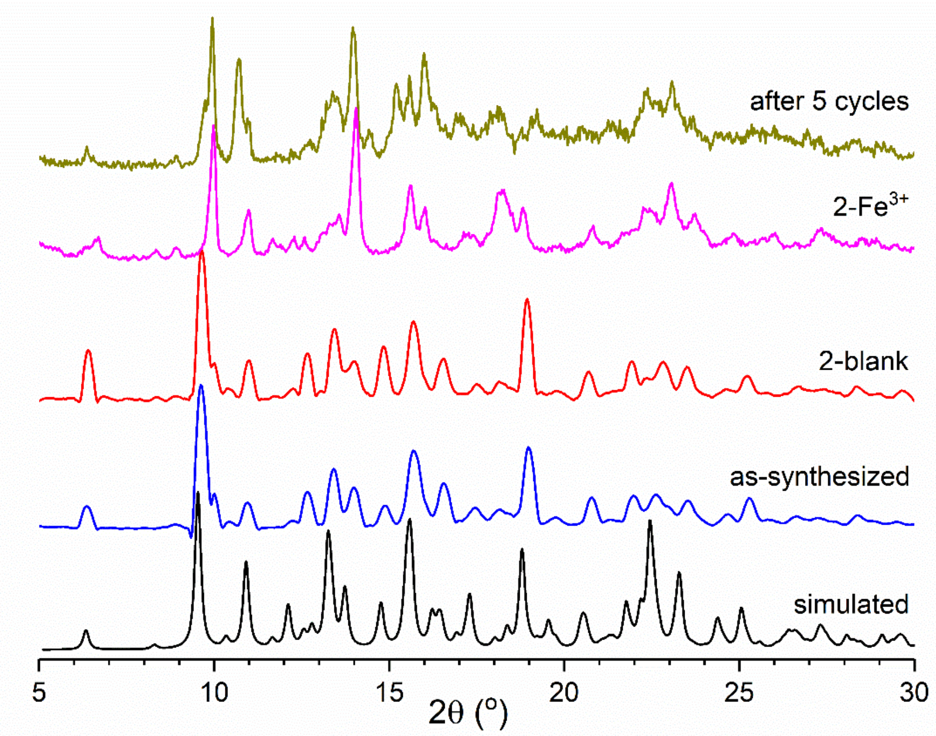


**(b).**

**Figure S21.** PXRD patterns before and after treatments with $Fe^{3+}$ ions for (a) **1** and (b) **2**.

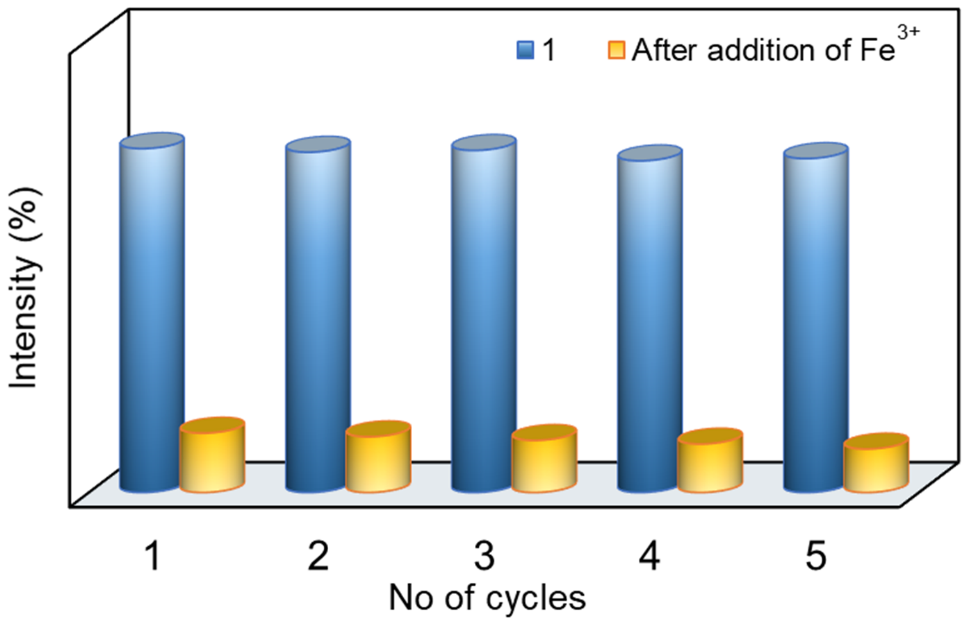


**(a).**

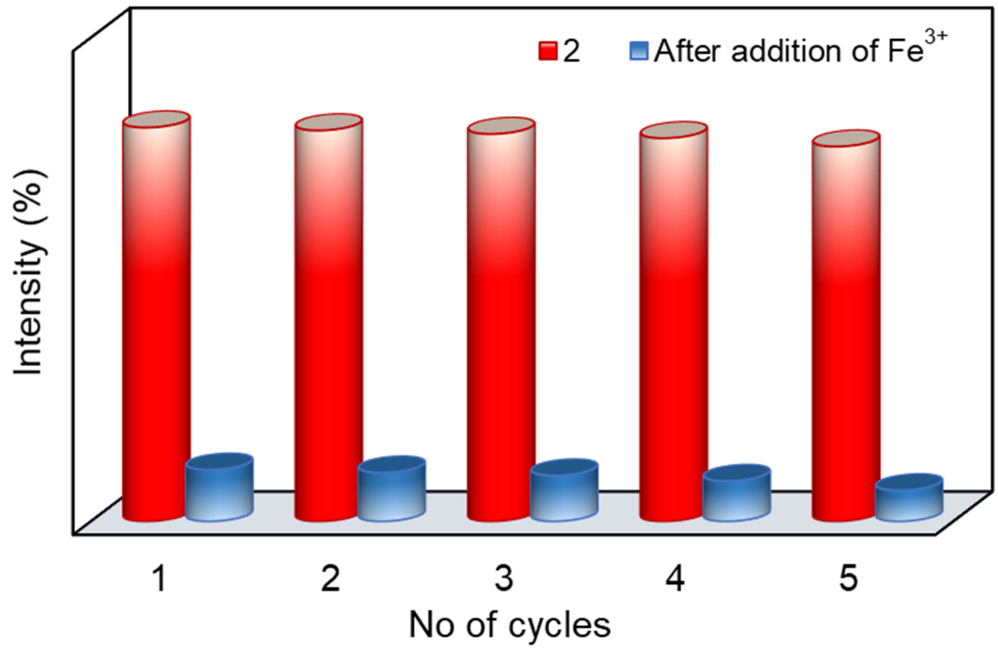


**(b).**

**Figure S22.** Bar diagrams showing the emission intensities of (a) **1** and (b) **2** treated with $Fe^{3+}$ for five repeated cycles.

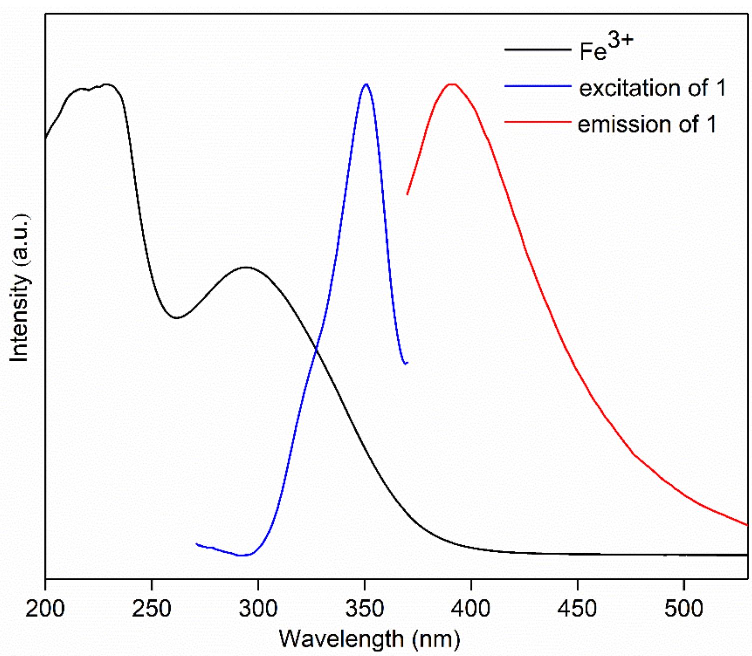


**(a).**

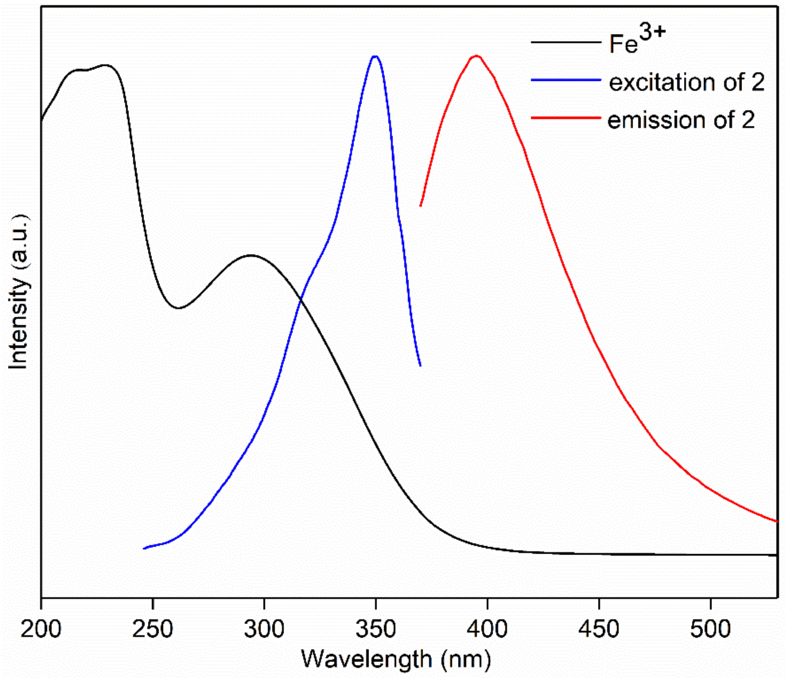


**(b).**

**Figure S23.** UV-vis absorption spectrum of $Fe^{3+}$ ions in aqueous solution and the excitation and emission spectra of (a) **1** and (b) **2**.

**Table S1.** Sensing properties of reported compounds toward various aromatic VOCs.

| Compound | Metal | $\lambda_{ex}$ | $\lambda_{em}$ | $[(I-I_0)/I_0]$ | Analytes | Reference |
|---|---|---|---|---|---|---|
| $[Zn(\mathbf{L})(1,4\text{-}NDC)\cdot H_2O]_n$, **1** | Zn | 350 | 403 | 1.91 | mesitylene | this work. |
| $[Cd(\mathbf{L})(1,4\text{-}NDC)(H_2O)\cdot MeOH]_n$, **2** | Cd | 350 | 406 | 1.65 | mesitylene | this work |
| NUS-1a | Zn | 400 | 504 | | benzene | J. Am. Chem. Soc. **2014**, *136*, 7241. |
| $Me_2NH_2)[Cd(TTCA)(H_2O)]\cdot 3DMF\cdot H_2O$ | Cd | 420 | 501 | 0.37 | m-xylene | Cryst. Growth Des. **2015**, *15*, 7, 3119. |
| In-bpy | In | 306 | 476 | 19.5 | p-xylene vapor | Chem. Eur. J. **2018**, *24*, 12474. |
| $Cd_3(L)(bipy)_2\cdot 4DMA$ | Cd | 324 | 427 | | benzene | **Mater. Horiz. 2015**, **2**, 245-251. |
| $[Zn_2(\mu_2\text{-}BDC)_2(iQ)_2]$ | Zn | 330 | 409 | 27.2 | p-xylene | *Crystals* **2020**, *10*, 5, 344. |
| NUS-40-Zn | Zn | 420 | 674 | 2.76 | o-xylene | Inorg. Chem. **2018**, *57*, 13631. |
| $[Cd_2(tppe)(bpdc)_2(H_2O)]$ | Cd | 380 | 496 | 0.90 | mesitylene | **Dalton Trans. 2016**, *45*, 14888-14892. |

**Table S2.** Sensing properties of reported compounds toward $Fe^{3+}$ions.

| Compound | Analytes | Stern-Volmer constant ($K_{sv}$, $M^{-1}$ ) | Adjusted $R^2$ | Limit of detection (μM) | Reference |
|---|---|---|---|---|---|
| $[Zn(L)(1,4\text{-}NDC)\cdot H_2O]_n$, **1** | $Fe^{3+}$ | 6.895 x $10^5$ | 0.997 | 2.35 | this work |
| $[Cd(L)(1,4NDC)H_2O\cdot MeOH]_n$,**2** | $Fe^{3+}$ | 9.940 x $10^5$ | 0.975 | 1.01 | this work |
| $[Zn_2(L)_2(bpe)_2(H_2O)_2]$ | $Fe^{3+}$ | 2.5 x $10^5$ | | 25 | **Dalton Trans. 2015**, ***44***, 18795-18803. |
| $\{[Cd_2(dpc)(bib)(H_2O)]\cdot H_2O\}n$ | $Fe^{3+}$ | 8.939 x $10^6$ | 0.974 | | Journal of S. S. Chemistry. **2019**, *277*, 564–574. |
| $[Bmim][Dy(NO_3)_4]$ | $Fe^{3+}$ | 2.0×$10^6$ | 0.982 | 9.4 | **Dalton Trans. 2016**, ***45***, 1040-1046. |
| **ZSTU-1** | $Fe^{3+}$ | 2.69×$10^6$ | 0.990 | 6.38 | Journal of S. S. Chemistry. **2019**, *278*, 120-892. |
| **$[Cd(L)(4\text{-}CPA)]_n$** | $Fe^{3+}$ | 3.866 × $10^5$ | 0.988 | 4.70 | Polyhedron. **2018**, *151*, 530-536. |
| $\{[Cd_4(HDDCP)_2(4,4'\text{-}bibp)_2(H_2O)_2]\cdot 2.5(DOA)\cdot 1.5(H_2O)\}_n$<br>$\{[Cd_2(HDDCP)(1,4\text{-}bib)(H_2O)]\cdot H_2O\}_n$ | $Fe^{3+}$ | 2.15 x $10^5$<br>8.86 x $10^4$ | 0.998<br>0.995 | 1.34<br>3.32 | **CrystEngComm 2020**, ***22***, 6927. |
| $\{[Zn(L)(dcdps)]\}n$<br>$\{Zn(L)(bdc)\}n$<br>$\{[Cd(L)(oba)]\cdot 0.5DMF\}_n$<br>$\{[Cd(L)(bdc)\cdot(H_2O)_2]\cdot 2DMF\}_n$ | $Fe^{3+}$ | 7.004 x $10^3$<br>9.066 x $10^3$<br>4.984 x $10^3$<br>6.387 x $10^3$ | 0.992<br>0.970<br>0.968<br>0.966 | 6.21<br>4.45<br>11.52<br>6.36 | Cryst. Growth Des. **2020**, *20*, 1898. |
| $[Zn_2(L_{13})_2(bpe)_2(H_2O)_2]_n$ | $Fe^{3+}$ | 2.39 x $10^3$ | | 2.50 | Dalton Trans. **2015**, *44*, 18795. |
| $[Zn(tpb)(Hbtc)]_n$ | $Fe^{3+}$ | 1.57 x $10^4$ | 0.998 | 1.95 | **Dalton Trans. 2020**, ***49***, 11201. |
| $\{[Zn(L1)(BTEC)0.5]\cdot 3.1H_2O\}_n$<br>$\{[Zn(L2)0.5(BTEC)0.5]\cdot 1.5H_2O\}_n$<br>$\{[Zn_2(L3)(BTEC)(H_2O)]\cdot H_2O\}_n$<br>$\{[Zn_2(L4)(BTEC)]\cdot H_2O\}_n$ | $Fe^{3+}$ | 5314<br>6775<br>6636<br>6424 | 0.994<br>0.990 | 6.35<br>5.01<br>7.02<br>6.19 | **CrystEngComm 2021**, ***23***, 1604. |
| $Eu^{3+}$@1 | $Fe^{3+}$ | 5.12 x $10^3$ | 0.999 | 0.5 | **J. Mater. Chem. A. 2014**, ***2***, 13691. |
| $\{[Cd(5\text{-}asba)(bimb)]\}_n$ | $Fe^{3+}$ | 1.78 x $10^4$ | | 1.87 | **J. Mater. Chem. C. 2016**, ***4***, 11404. |
| $\{[Zn_2(1,4\text{-}ndc)_2(3\text{-}abpt)]\cdot 2DMF\}_n$<br>$\{[Cd(1,4\text{-}ndc)(3\text{-}abit)]\cdot H_2O\}_n$ | $Fe^{3+}$ | 2.38 x $10^4$<br>9.54 x $10^3$ | 0.992<br>0.993 | | **New J. Chem. 2017**, ***41***, 8107. |
| $[Zn_2(oba)_2(bpta)]\cdot 3DMF\}_n$ | $Fe^{3+}$ | 6.50 x $10^4$ | 0.990 | 3.00 | Polyhedron. **2019**, *166*, 166. |